The Irminger Gyre as a Key Driver of the Subpolar North Atlantic Overturning

A. Sanchez-Franks[1] , N. P. Holliday[1] , D. G. Evans[1] , N. Fried[2] , O. Tooth[3] , L. Chafik[4] , Y. Fu[5] , F. Li[6], M. F. de Jong[2] , and H. L. Johnson[3]

[1]National Oceanography Centre, Southampton, UK, [2]NIOZ, Royal Netherlands Institute for Sea Research, Texel, The Netherlands, [3]Department of Earth Sciences, University of Oxford, Oxford, UK, [4]Department of Meteorology, Stockholm University, Stockholm, Sweden, [5]School of Earth and Atmospheric Sciences, Georgia Institute of Technology, Atlanta, GA, USA, [6]State Key Laboratory of Marine Environmental Science, Xiamen University, Xiamen, China

Abstract The lower limb of the Atlantic meridional overturning circulation (AMOC) is the equatorward flow of dense waters formed through the cooling and freshening of the poleward-flowing upper limb. In the subpolar North Atlantic (SPNA), upper limb variability is primarily set by the North Atlantic Current, whereas lower limb variability is less well understood. Using observations from a SPNA mooring array, we show that variability of the AMOC's lower limb is connected to poleward flow in the interior Irminger Sea. We identify this poleward flow as the northward branch of the Irminger Gyre (IG), accounting for 55% of the AMOC's lower limb variability. Over 2014–2018, wind stress curl fluctuations over the Labrador and Irminger Seas drive this IG and AMOC variability. On longer (>annual) timescales, however, an increasing trend in the thickness of intermediate water, from 2014 to 2020, within the Irminger Sea coincides with a decreasing trend in IG strength.

Plain Language Summary In the subpolar North Atlantic, warm salty waters get transported northwards by the upper branch of the meridional overturning circulation. As they travel northwards, they transform: cooling, densifying, and sinking. The cooler deeper waters then get transported back southwards toward the equator in the lower branch of the overturning circulation. The transformation and transport of these waters plays a critical role in our climate system. However, the lower branch of the overturning circulation and the mechanisms controlling how it changes are still not well understood. Observations from a fixed array of moorings between Greenland and Scotland are used here to identify the interior (away from land boundaries) Irminger Sea as a region important for the overturning's lower branch. Specifically, we find that a closed system of currents in the western Irminger Sea, known as the Irminger Gyre, plays an important role in the overturning's variability. Gyre strength is then linked to the recirculation of newly transformed waters that get exported as part of the overturning's lower branch. Finally, we investigate the impact of the atmosphere on Irminger Sea circulation and find that fluctuations of the winds are important drivers of change in this gyre and the overturning.

1. Introduction

The Atlantic meridional overturning circulation (AMOC) is key in regulating the global climate system due to its role in heat and freshwater transport (Srokosz et al., 2012). In the subpolar North Atlantic (SPNA), the light waters of the AMOC's upper limb are densified by water mass transformation and subsequently exported equatorward in the AMOC's lower limb (Brambilla et al., 2008; Desbruyères et al., 2019). The formation and ventilation of dense water within the lower limb also sequesters carbon via the subduction of CO_2-rich surface waters, and thus represents an important carbon sink in the climate system (Fontela et al., 2016; Sabine et al., 2004).

The Overturning in the Subpolar North Atlantic Programme (OSNAP) is a trans-basin ocean observing array that has been providing direct observations of the SPNA AMOC since 2014. The array stretches across the SPNA, spanning Scotland to Greenland (OSNAP East, Figure 1a) and Greenland to Labrador (OSNAP West). One of the key findings of the OSNAP project is that water mass transformation in the eastern subpolar gyre at OSNAP East dominates the strength and variability of the AMOC in the SPNA compared to OSNAP West (Li et al., 2021; Lozier et al., 2019). This is contrary to previous work that suggested convection in the Labrador Sea sets the variability and strength of the SPNA AMOC (Medhaug et al., 2012; Thornalley et al., 2018). Direct observations have determined that monthly to interannual AMOC variability across OSNAP East is not constrained to a single
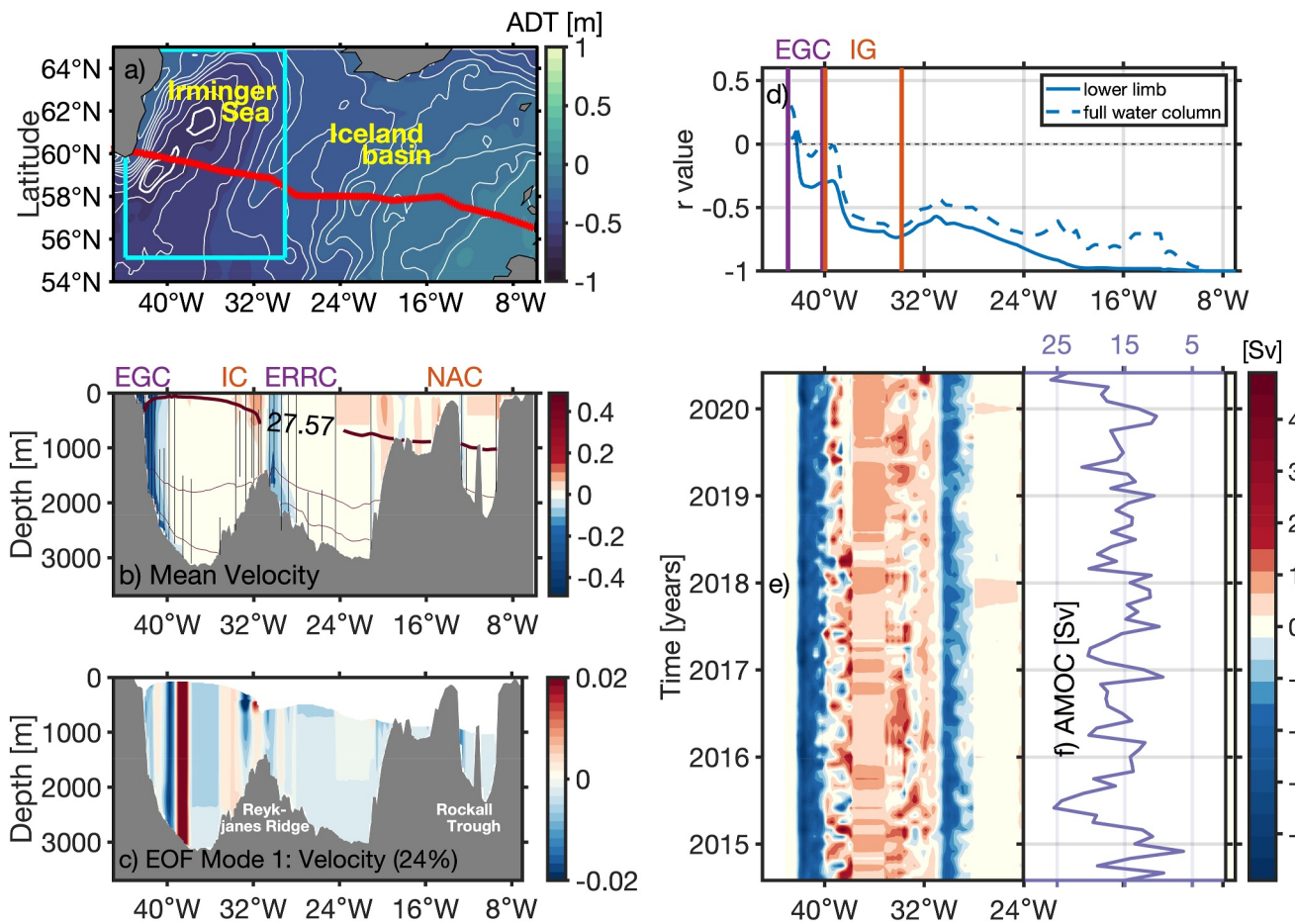
Figure 1. (a) Absolute Dynamic Topography (ADT (m)) over the eastern subpolar gyre. Red line indicates the location of the Overturning in the Subpolar North Atlantic Programme (OSNAP) East array. (b) Mean velocity field across OSNAP East. Isopycnals contoured in black, with mean isopycnal of maximum overturning (27.57 kg m^{-3}) in bold. Vertical black lines indicate mooring locations. (c) Empirical orthogonal function mode 1 of velocity variations in the lower limb across OSNAP East, calculated using the mean value of the isopycnal of maximum overturning 27.57 kg m^{-3} to define the lower limb. (d) Correlation between the Atlantic meridional overturning circulation (AMOC) and the volume transport accumulated eastward along OSNAP East at each longitude. (e) Hovmöller diagram of the vertically integrated volume transport of the lower limb across OSNAP East, with the time series of the AMOC embedded (f) for comparison. In July 2018, a mooring was removed from the interior western Irminger Sea, apparent in panel (e); hence for (b–d) only the 2014–2018 OSNAP period was used. EGC = East Greenland Current, IC = Irminger Current, ERRC = East Reykjanes Ridge Current, NAC = North Atlantic Current, LSW = Labrador Sea Water, NEADW = North East Atlantic Deep Water, DSOW = Denmark Straits Overflow Water, and ISOW = Iceland-Scotland Overflow Water. IG = Irminger Gyre.

region but is spread across the western boundary current (i.e., East Greenland Current (EGC)), as well as the Irminger and Iceland basins (Li et al., 2021). However, satellite and model hindcast simulations have shown that the Irminger Sea is a key region for AMOC variability on interannual to decadal time scales (Chafik et al., 2022; Megann et al., 2021).

The Irminger Sea is a climatically important region. At the eastern boundary of the Irminger Sea, the Irminger Current (IC, Fried & de Jong, 2022) transports warm waters northward. As the IC progresses poleward past the OSNAP array, it splits, with one branch continuing northward into the Nordic Seas and the other branch returning southward and eventually joining the cooler fresher waters of the EGC (Pickart et al., 2005). Along the western boundary of the OSNAP East array (Figures 1a and 1b), the equatorward flowing EGC advects cool and fresh Arctic-origin waters. In the interior of the Irminger Sea, a narrow cyclonic gyre, known as the Irminger Gyre (IG), circulates in the western side of the basin (Figure 1a, Lavender et al., 2000; Våge et al., 2011). The IG is largely barotropic and at mid-depths is found to contain Labrador Sea Water (LSW, Våge et al., 2011). The origin of LSW in the Irminger Sea has been traced to local convection (Våge et al., 2011; van Aken et al., 2011) as well as remote formation (i.e., the Labrador Sea) where the IG provides a connection between the Labrador and Irminger Sea (Faure & Speer, 2005; Straneo et al., 2003; Talley & McCartney, 1982). The variability of the IG has been linked

to cyclonic wind stress curl (WSC) off the eastern coast of Greenland on seasonal to interannual timescales in ocean models (Spall & Pickart, 2003).

While the Irminger Sea has been recently highlighted as an important region for AMOC variability on interannual to decadal timescales (e.g., Chafik et al., 2022; Megann et al., 2021), the connection between the Irminger Sea and the AMOC is unexplored on shorter timescales. Further, several studies have shown buoyancy forcing is an important mechanism for the AMOC on lower frequencies (interannual to decadal) (Yeager et al., 2021), but there is a gap in our understanding of driving mechanisms for shorter timescales especially those captured by observations (e.g., Jackson et al., 2022). Thus, we use direct observations from the OSNAP mooring array to investigate the role of the interior Irminger Sea in the variability of the AMOC (Section 3). We identify the dominant features of the interior Irminger Sea pathways that govern AMOC variability (Section 4) and examine the density and atmospheric fields that potentially drive this variability of interior Irminger Sea circulation (Sections 5 and 6).

2. Data and Methods

2.1. The OSNAP Mooring Data

The OSNAP array is constructed from moored temperature, salinity and current meters, autonomous profilers, and hydrographic sections (Li et al., 2017; Lozier et al., 2019).

The velocity and property fields are interpolated onto a regular grid along the OSNAP section using monthly means from 2014 to 2020 (Fu et al., 2023b). The grid has a horizontal and vertical resolution of $\frac{1}{4}°$ and 20 m, respectively. The property fields, that is, temperature, salinity, and density, are interpolated within the boundary currents where the mooring data exists. In the interior, property fields are estimated in the upper 2,000 m via an objective analysis method (further details in Li et al., 2017) using autonomous profilers (i.e., Argo floats and gliders), mooring data, and the WOA 2013 climatology (Locarnini et al., 2013; Zweng et al., 2013). Below 2,000 m, in the interior, hydrographic data from research expeditions in 2014 and 2016 are used. Similarly, the velocity field is estimated from mooring velocity data at the boundary currents, while in the surface Ekman layer, ERA5 reanalysis wind stress is used (Hersbach et al., 2020), and geostrophic velocities in the interior come from dynamic height (moorings) and altimetry (Li et al., 2017). We note that after June 2018, a mooring (M5) on the western side of the interior Irminger Sea was removed from the array, impacting the estimate of mass transport in that region and strengthening the mean AMOC by 0.4 Sv (Fu et al., 2023b); hence, throughout this manuscript, the 2014–2018 period is used when calculating correlations.

Data from the OSNAP timeseries are supplemented with absolute dynamic topography (ADT) data from Copernicus Marine Environment Monitoring Service gridded multimission satellite altimetry, and wind stress data from ERA5 (Hersbach et al., 2020). Both data sets have a $\frac{1}{4}°$ resolution in space and monthly in time.

2.2. Volume Transport Calculations

In the SPNA, density surfaces slope strongly across the basin. Because of this, the AMOC is measured in terms of density coordinates and can be considered the transformation of light waters associated with the upper limb to denser water transported by the lower limb. Thus, the AMOC is defined here as the maximum of the overturning streamfunction, $\Psi(\sigma, t)$, in density coordinates (Lozier et al., 2019), where v is the volume transport (per unit length in the zonal direction per unit density) perpendicular to the OSNAP array, integrated from west (x_w) to east (x_e) across OSNAP East, and from the surface ($\sigma_{\min}$) through to all density surfaces:

$$AMOC(t) = \max[\Psi(\sigma, t)] = \max\left[\int_{\sigma_{\min}}^{\sigma} \int_{x_w}^{x_e} v(x, \sigma, t) dx d\sigma\right], (Sv) \tag{1}$$

Over the 2014–2020 period, the mean value of the isopycnal of maximum overturning (σ_{MOC}), separating the upper and lower limbs, across OSNAP East is 27.57 kg m^{-3} (Figure 1b). The lower limb is defined as the transport component between the sea floor and the time-varying $\sigma_{MOC}(t)$. Throughout the text, all reference to the AMOC and the AMOC lower limb is for OSNAP East only, unless stated otherwise. When computing correlations, the statistical significance is determined using the effective degrees of freedom calculated as the length of each time series over the integral timescale of decorrelation (Emery & Thomson, 2001).

3. The Interior Irminger Sea and the AMOC's Lower Limb

The key circulation features of the lower limb are the denser component of the southward flowing EGC, a northwards flow in the western interior Irminger Sea, the overflow waters beneath the northward IC, and the southwards flowing East Reykjanes Ridge Current (ERRC, Figure 1b). An empirical orthogonal function (EOF) analysis of the OSNAP East velocity field shows that most of the variability across the lower limb is concentrated in the western interior Irminger Sea, and weaker secondary regions of variability in the IC and the ERRC (Figure 1c). The principal component (PC1) time series associated with EOF Mode 1 has a correlation of $r = -0.41$ (statistically significant at the 95% level) with the AMOC, suggesting that variability in the Irminger Sea is linked to changes in the AMOC.

The connection between the AMOC and circulation in the Irminger basin is further investigated via the correlation as a function of longitude between the AMOC and the accumulated volume transport integrated from the westernmost point of the OSNAP East array eastward (Figure 1d). In the region of the EGC, correlation values are $r = -0.33$ for the accumulated transport and the AMOC lower limb. This weak correlation between the AMOC and the western boundary current is consistent with findings by Li et al. (2021) who showed that the EGC accounts for only 10% of AMOC variability at OSNAP East. Moving in the eastward direction there is an abrupt increase in correlation within the western and central interior Irminger Sea, a region shown here to be dominated by northward flow and strong variability (Figures 1b and 1e), with a correlation of up to $r = -0.75$ and $r = -0.67$ (statistically significant at the 95% level) for the lower limb and the full water column transport, respectively (Figure 1d). We note this correlation decreases slightly to $r = -0.65$ when the AMOC is calculated over the full OSNAP (East and West) section. The correlation decreases over the regions of the IC and the ERRC. The low correlation between the AMOC and the boundary currents (i.e., the EGC or IC) may be due to differences in the dominant frequencies of variability associated with the topography of the basin (Hopkins et al., 2019).

A Hovmöller diagram of the vertically integrated volume transport in the lower limb at each longitudinal grid point across OSNAP East shows a strong and highly variable northward flow in the interior western Irminger Sea (Figure 1e), coincident with the region of high correlation shown in Figure 1d. The correlation between the AMOC and the time-varying northward flow east of 40°W highlights that an increase in this northward transport coincides with a weakening of the AMOC (Figures 1e and 1f). We note that there is no mooring data in the eastern portion of the interior Irminger Sea (Figure 1b), so geostrophic velocity is calculated from the tall moorings bounding this region. This manifests as a band of lower magnitude variability and lower spatial resolution in this region (Figure 1e).

In this section, we have shown that the western interior Irminger Sea is a hotspot of SPNA AMOC variability, associated with the northward flow in this region. The circulation within the western interior Irminger Sea and its connection to the AMOC are further explored in the next section.

4. The Cyclonic Circulation of the Irminger Sea

The northward transport in the interior Irminger Sea is investigated here via composites of the velocity field and ADT during time periods of strong and weak AMOC (Figure 2). During periods when the AMOC is strong (i.e., greater than one standard deviation above the mean AMOC), there is extremely weak northward transport in the interior Irminger Sea (Figure 2a). The velocity field also shows a weak bottom-intensified southward velocity core east of 40°W, corresponding to an eastward shift of the deepest core of the Deep Western Boundary Current (Hopkins et al., 2019). Conversely, when the AMOC is weak (i.e., less than one standard deviation below the mean, Figure 2b), there is a strengthening of the northward flow in the western interior Irminger Sea. Composites of the ADT during strong/weak AMOC periods show a closed cyclonic circulation in the western Irminger Sea. When the AMOC is strong, this gyre expands, and when the AMOC is weak, this gyre contracts (Figures 2c and 2d). The ADT across the OSNAP line also shows a steepening of its gradient in the western interior Irminger Sea during the weak AMOC period (Figure 2e), consistent with the contraction of this gyre and the strengthening of the northwards flow in the interior Irminger Sea, and vice versa. We identify this cyclonic circulation in the western Irminger Sea as the IG, and the northwards flow in the western interior Irminger Sea as its northwards flowing branch.

The northward branch of the cyclonic IG, hereafter referred to as the IG, has been previously reported as a weakly baroclinic flow in the mean field (Käse et al., 2001; Lavender et al., 2000; Våge et al., 2011). Here, the IG is a
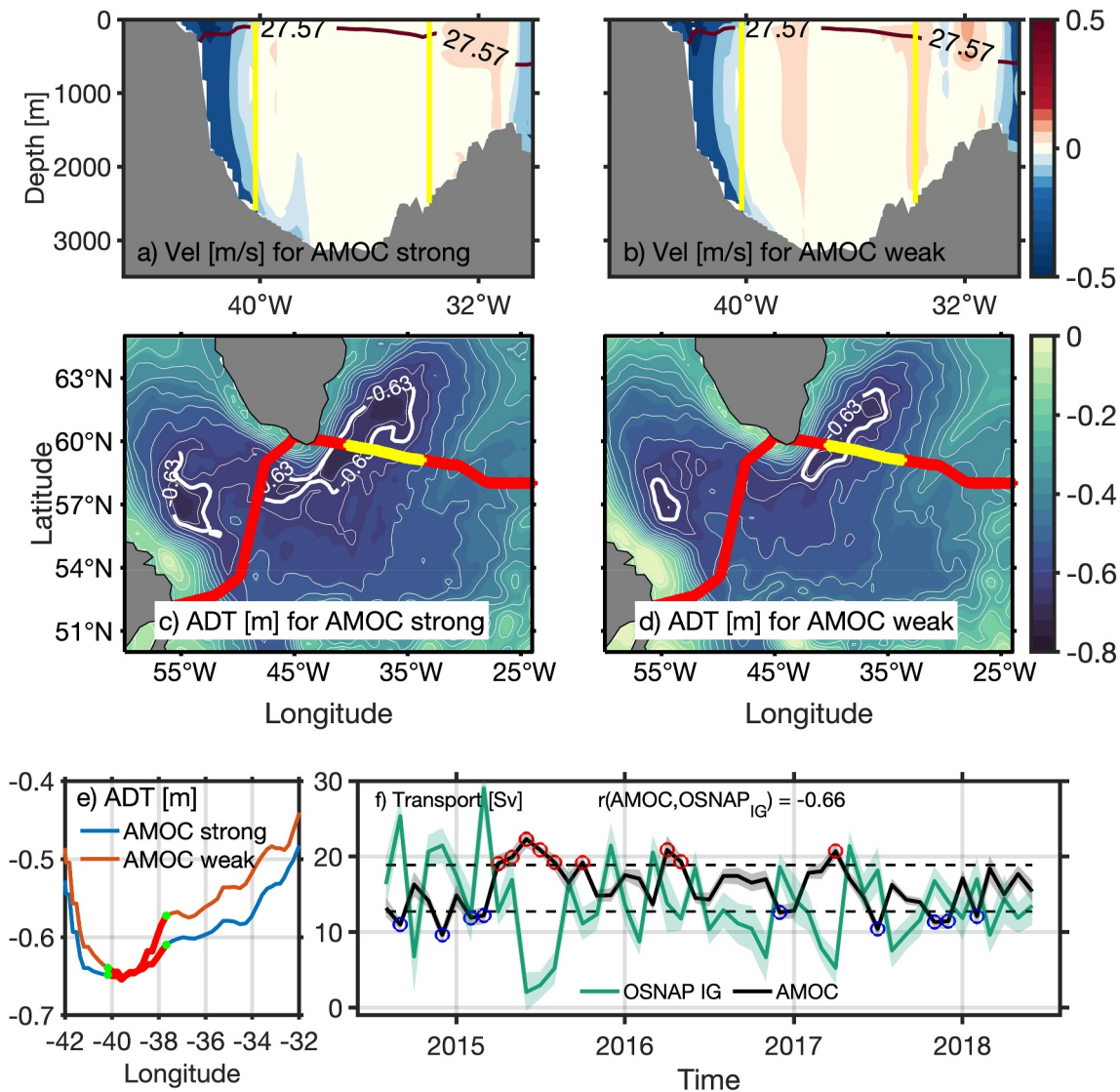
Figure 2. Composites of mean velocity in the interior Irminger Sea during (a) Atlantic meridional overturning circulation (AMOC) strong and (b) AMOC weak periods. (c, d) Same as in (a, b) but for absolute dynamic topography (ADT) over the subpolar North Atlantic. Red line in panels (c, d) indicates the location of Overturning in the Subpolar North Atlantic Programme (OSNAP) array, while yellow line indicates the span of the interior Irminger Sea, corresponding to yellow lines in panels (a, b). ADT contours are shown at 0.05 m intervals. (e) ADT over the Irminger Sea along OSNAP line for AMOC strong and weak periods. AMOC strong periods are defined as events one standard deviation above the mean AMOC value, and vice versa. (f) Volume transport of the Irminger Gyre (green line) compared with the AMOC from OSNAP East (black line). Red and black circles in panel (f) indicate AMOC strong and weak periods, respectively. Correlation is significant at 99% level. Shading indicates monthly uncertainty estimates using a Monte Carlo technique.

persistent feature east of 40°W, varies strongly with time (Figures 1e and 2f), and has a predominantly intra-seasonal timescale (peaking at 3 months; Figure S1b in Supporting Information S1). Spectral analysis of the AMOC and IG suggests higher energy at intraseasonal timescales with relatively lower energy at a period of 1 year (Figure S1 in Supporting Information S1). The seasonal climatology of the IG and the AMOC (Figure S2 in Supporting Information S1) confirms that the IG does not appear to have a strong seasonal signal, consistent with Spall and Pickart (2003), while the AMOC does have some seasonality, consistent with Fu et al. (2023a, 2023b). Removing lower frequency ($\geq$12 months) variability from the AMOC and IG time series (Figure S3 in Supporting Information S1) does not significantly alter our results, suggesting that intra-annual variability is the most relevant timescale for these processes.

The IG transport, defined here as the volume transport between 40°10′W-33°47′W following limits in Figure 1d, has a mean northward transport of 14.39 Sv and a correlation of $r = -0.66$ (statistically significant at 95% level)

with the monthly AMOC time series over 2014–2018, suggesting that strengthening of the IG transport coincides with a weakening of the AMOC's net southward transport, and vice versa (Figure 2), consistent with Section 3. We also note that the IG's correlation with the AMOC across the full OSNAP array (i.e., OSNAP West and East) increases to $r = -0.69$. Mean values of the northward limb of the IG have been reported at ∼7 Sv, when the IG is defined strictly as the flow in the western interior Irminger Sea (Våge et al., 2011). Similarly, here we find that if we restrict our definition to the western interior Irminger Sea (∼40°–37.5°W), the mean transport reduces to ∼5.5 Sv, consistent with the previously reported values.

The dynamics of the IG are key in setting the variability of the SPNA AMOC by affecting the strength of the northward flow within the western interior Irminger Sea. In the next section, the Irminger Sea density field is examined as a potential driver of IG variability.

5. The Irminger Gyre and the Intermediate Water Masses of the Subpolar North Atlantic

LSW is a widespread intermediate water mass in the SPNA, formed within the Labrador and Irminger Seas (de Jong & de Steur, 2016; Pickart et al., 2003; Yashayaev et al., 2007). The density range of LSW is typically 27.7–27.8 kg m^{-3} in the Irminger Sea (Holliday et al., 2018) as shown across the lower limb of OSNAP East in Figure 3.

In the interior Irminger Sea and the IG we observe a potential vorticity (PV) minimum bounded by the 27.7–27.8 kg m^{-3} isopycnals (Figure 3b). PV minima at this depth in the Irminger Sea have been previously used by Pickart et al. (2003) to identify the presence of LSW. Recently, a more detailed description of the water masses in the western Irminger Sea has identified Upper Irminger Sea Intermediate Water (UISIW) and Deep Irminger Sea Intermediate water (DISIW) (Le Bras et al., 2020). UISIW forms near the boundary current with a density range of 27.65–27.73 kg m^{-3}. DISIW is formed in the interior (around 40°W) with a density range of 27.73–27.77 kg m^{-3} and is associated with a local salinity and PV minimum. Temperature-salinity (T-S) profiles within the western interior Irminger Sea highlight an absolute salinity minimum of ∼35.02 g kg^{-1} with a mean conservative temperature of ∼3.4°C along the 27.74 kg m^{-3} isopycnal (Figure 3c), consistent with the DISIW. The T-S properties show that the low PV DISIW is mostly present where we observe the northwards velocity of the IG (and to a lesser extent southward velocity, likely corresponding to the EGC) (Figure 3c).

Over the OSNAP period, the density structure shows a significant increase in volume of the DISIW over time (Figures 3d and 3f), primarily through the shoaling of the 27.74 kg m^{-3} isopycnal (Figure 3d). The layer thickness between the 27.74 and 27.8 kg m^{-3} isopycnal increases by 480 m over 6 years (Figure 3f). The increasing trend in the deep intermediate water mass suggests that the OSNAP data capture a period of enhanced convection, consistent with de Jong and de Steur (2016). We observe a concurrent decreasing trend in the IG transport over the same period, with a reduction of 4 Sv over 6 years. This is consistent with the hypothesis of Våge et al. (2011) where an increase in volume of intermediate water masses in the interior Irminger Sea causes a decrease in IG velocity on interannual timescales. Fried and de Jong (2022) also found that changes in the gradient of the density field across the Irminger Sea contribute to transport variability in this region (e.g., increases in the density gradient result in higher volume transport). Further, Chafik et al. (2022) have shown that changes in the Irminger Sea density field are linked to AMOC variability on interannual to decadal timescales. However, we find no statistically significant trend in the AMOC time series over 2014–2020 or statistically significant correlation between the LSW (DISIW in particular) layer thickness in the Irminger Sea and the AMOC on shorter (<annual) timescales.

In this section, we examined the density field as a potential driver of IG variability and found a connection between the trends in IG transport and intermediate water mass thickness. Next, we examine whether atmospheric forcing provides a mechanistic explanation for the correlation between the northward transport of the IG and AMOC variability discussed in Section 4.

6. Atmospheric Drivers of the Irminger Gyre and AMOC Variability

In the subpolar gyre, strong westerly winds and increased frequency of westerly Greenland tip jets (Våge et al., 2009) are characteristic of positive North Atlantic Oscillation (NAO) conditions (Rogers, 1990). Over the 2014–2018 OSNAP period, NAO positive conditions persisted over the SPNA. During this period, deep
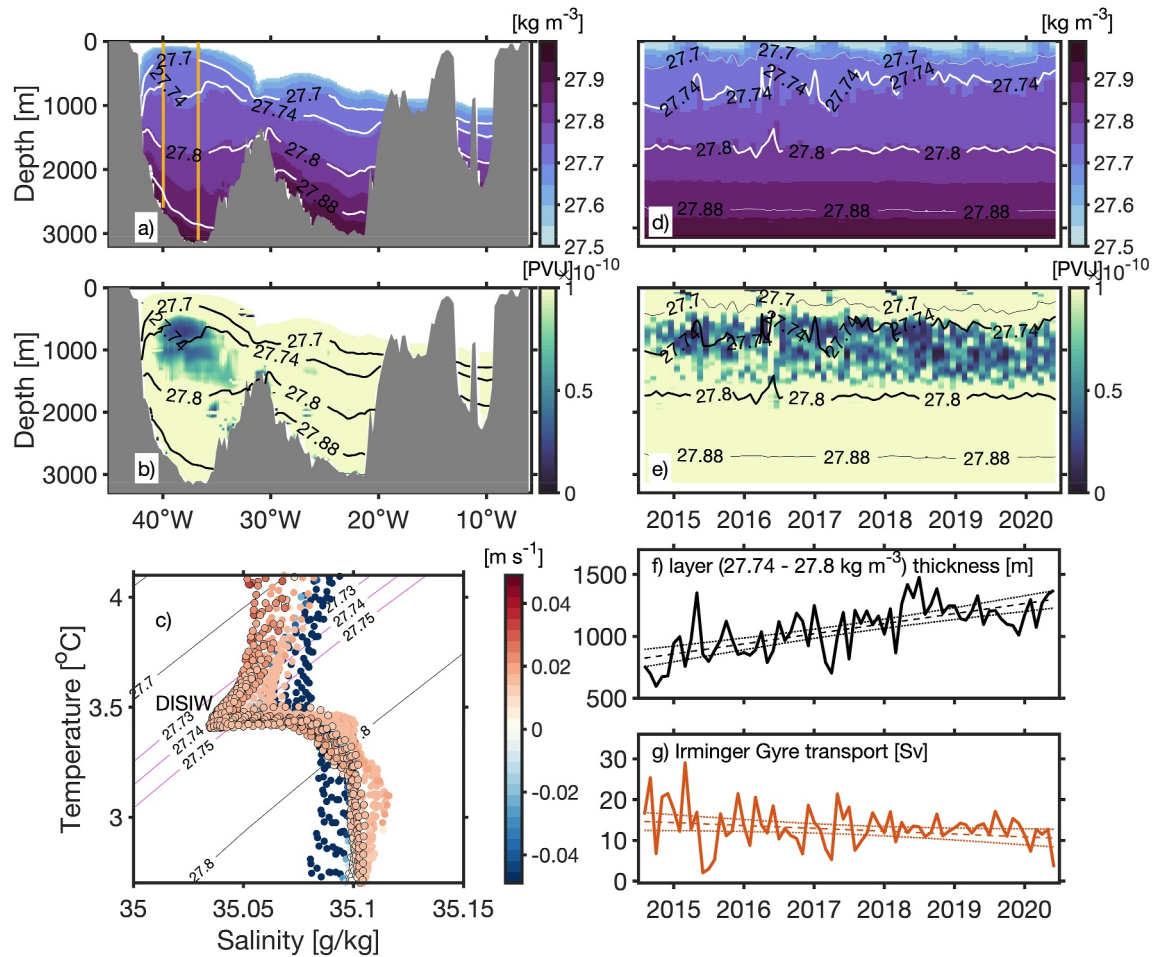
Figure 3. Mean (2014–2020) (a) density and (b) potential vorticity (PV) across the lower limb of Overturning in the Subpolar North Atlantic Programme (OSNAP) East, defined using the mean value of the isopycnal of maximum overturning, 27.57 kg m^{-3}. (c) Conservative temperature and absolute salinity diagram of the time-averaged profiles at every longitude point between the East Greenland coast and the eastern limit of the Irminger Gyre (IG) (easternmost yellow line in panel (a)); profiles are colored by velocity (m s^{-1}) and data points outlined in black indicate profiles from IG region. The pink lines show the isopycnals that correspond to the Deep Irminger Sea Intermediate water (DISIW) in the region of interest. Temporal evolution of the (d) density and (e) PV in the zonally averaged IG region (yellow lines in panels (a, b)) indicating an increase in lower intermediate waters over time. Time series and trends of the DISIW layer (27.4–27.8 kg m^{-3}) (f) thickness and (g) IG transport over OSNAP period. Dotted lines in panels (f, g) indicate 95% confidence intervals.

convection occurred within the Labrador Sea, south of Cape Farewell, and in the Irminger Sea (de Jong & de Steur, 2016; de Jong et al., 2018; Piron et al., 2017; Zunino et al., 2020). This convection was coincident with regions of positive WSC (Figure 4a). Strong westerlies dominate the SPNA while northeasterlies affect the eastern coast of Greenland (Figure 4a). We observe positive WSC across most of the Labrador Sea and the eastern subpolar gyre, and negative WSC across the eastern North Atlantic south of 56°N.

A comparison between the OSNAP-derived IG transport and the WSC in the SPNA for the 2014–2018 positive NAO period reveals a region of strong positive correlation (maximum value of $r = 0.62$ in the Irminger Sea, statistically significant at 95% level) over the Labrador and Irminger Seas (Figure 4b), in regions where the time-mean WSC is positive (Figure 4a). This suggests that an increase in the WSC over the Labrador and Irminger Seas leads to a strengthening of IG transport, and vice versa. In general, strong WSC over the Labrador and Irminger Seas acts to spin up the interior circulation, thus connecting the IG and the Labrador Sea (e.g., Faure & Speer, 2005; Lavender et al., 2000). Here, we find that WSC over the Labrador and Irminger Seas drives IG variability, as calculated from OSNAP data. We also note that although we have focused on the OSNAP-derived northward branch of the IG, we expect this relationship to apply to the whole gyre; further investigation is needed to confirm these mechanisms.
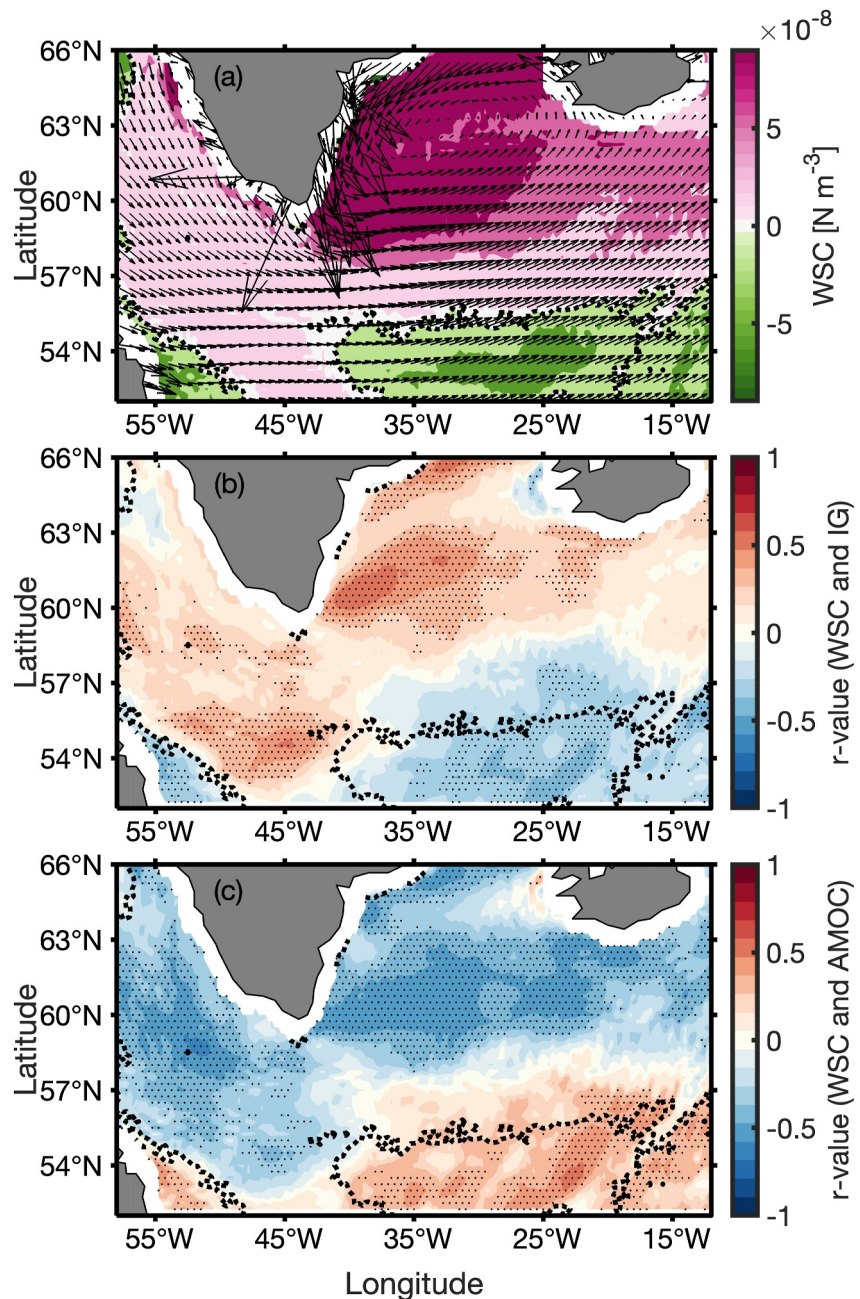
Figure 4. (a) Wind stress (vectors) and wind stress curl (WSC) (contours) over the 2014–2018 positive North Atlantic Oscillation period (December 2014–October 2018). Correlation between the WSC and the Irminger Gyre transport at (b) the Overturning in the Subpolar North Atlantic Programme array and (c) the Atlantic meridional overturning circulation. Black dotted contour (a–c) indicates the zero WSC line. Stippling in panels (b, c) indicates statistical significance at 95% level.

Conversely, the pattern of correlation between the AMOC and WSC across the SPNA shows negative values over the Labrador and Irminger Seas (maximum value $r = -0.60$), suggesting a strengthening of the WSC is linked to a weakening of the AMOC (Figure 4c). Correlation values between the WSC and the AMOC across the full OSNAP (West and East) section shows similar patterns, with maximum correlation values increasing slightly to $r = -0.61$. The connections between the WSC and the IG and AMOC are consistent with the mechanism suggested in Section 4, that is, where a strengthening IG drives a weaker AMOC. Thus, increased WSC east of Greenland and over the Irminger Sea acts to strengthen the IG, increasing the northward flow within the western interior Irminger Sea. This increased northward flow subsequently decreases the net southward transport of the

AMOC. We note that the max correlations between the WSC and the IG or AMOC weaken (r = 0.48, 0.37, respectively) for the full OSNAP period, 2014–2020, and maximum correlations between WSC and IG and AMOC weaken (r = 0.56, −0.55, respectively) when reconstructing the IG and AMOC timeseries without the Irminger Sea M5 mooring. Further investigation with a longer timeseries is needed to better understand these links.

Thus, here we have determined that fluctuations in WSC play a key role in driving AMOC variability during a persistent positive NAO event. These results are consistent with previous studies that have suggested that wind forcing is important on intra-annual timescales (e.g., Buckley & Marshall, 2016; Jackson et al., 2022).

7. Summary

In the SPNA, the Irminger Sea has been shown to be a climatically important region and a key driver of variability for the AMOC on interannual to decadal timescales (Chafik et al., 2022; Megann et al., 2021). Observational studies have further found that variability of the AMOC's lower limb is not constrained to a single region within the eastern subpolar gyre, but rather is spread over the western boundary, Irminger and Iceland basin on monthly to interannual timescales (Li et al., 2021).

In this study, we use data from a trans-basin mooring array to show that the Irminger Sea is a key region, or hotspot, of variability for the AMOC over the OSNAP period on shorter (intra-annual) timescales. We find that it is the IG that dominates the variability of the AMOC's lower limb with a correlation of r = −0.75 (accounting for over 55% of its variability), where strengthening in the northward limb of the IG coincides with weakening of the AMOC, and vice versa. Fluctuations in Irminger Sea density and local WSC are investigated as drivers of IG variability. We find that the trend in the IG is linked to the presence and recirculation of Irminger Sea intermediate waters (i.e., DISIW), highlighted by a similar trend in DISIW thickness at OSNAP. However, it is the fluctuations in WSC over the Labrador and Irminger Seas that dominate IG and AMOC variability over the OSNAP period, where strengthening of the WSC over the Labrador and Irminger Seas drives strengthening in the IG and weakening of the AMOC. This relationship between the IG-AMOC and WSC was observed during a period of persistent positive NAO. We also found all results hold when OSNAP West is included in the calculation of the AMOC time series.

In brief, we have used direct observations to demonstrate that wind stress is important to the IG-AMOC system over the OSNAP period on shorter (intra-annual) timescales, while buoyancy forcing is more likely to dominate on longer (>annual) timescales, consistent with findings in Jackson et al. (2022).

Data Availability Statement

The OSNAP data can be accessed here: https://www.o-snap.org/data-access/ (Fu et al., 2023a). Absolute dynamic topography from the Copernicus Marine Environment Monitoring Service gridded multimission satellite altimetry can be accessed from http://marine.copernicus.eu. The product used here, ID: SEALEVEL_GLO_PHY_L4_REP_OBSERVATIONS_008_047, was replaced in January 2022 with SEALEVEL_GLO_PHY_L4_MY_008_047 (European Union-Copernicus Marine Service, 2023).

References

Brambilla, E., Talley, L. D., & Robbins, P. E. (2008). Subpolar mode water in the northeastern Atlantic: 2. Origin and transformation. *Journal of Geophysical Research*, *113*(C4), C04026. https://doi.org/10.1029/2006JC004063

Buckley, M. W., & Marshall, J. (2016). Observations, inferences, and mechanisms of the Atlantic meridional overturning circulation: A review. *Reviews of Geophysics*, *54*(1), 5–63. https://doi.org/10.1002/2015RG000493

Chafik, L., Holliday, N., Bacon, S., & Rossby, T. (2022). Irminger Sea is the center of action for subpolar AMOC variability. *Geophysical Research Letters*, *49*(17), e2022GL099133. https://doi.org/10.1029/2022gl099133

de Jong, M. F., & de Steur, L. (2016). Strong winter cooling over the Irminger Sea in winter 2014–2015, exceptional deep convection, and the emergence of anomalously low SST. *Geophysical Research Letters*, *43*(13), 7106–7113. https://doi.org/10.1002/2016gl069596

de Jong, M. F., Oltmanns, M., Karstensen, J., & de Steur, L. (2018). Deep convection in the Irminger Sea observed with a dense mooring array. *Oceanography*, *31*(1), 50–59. https://doi.org/10.5670/oceanog.2018.109

Desbruyères, D. G., Mercier, H., Maze, G., & Daniault, N. (2019). Surface predictor of overturning circulation and heat content change in the subpolar North Atlantic. *Ocean Science*, *15*(3), 809–817. https://doi.org/10.5194/os-15-809-2019

Emery, W. J., & Thomson, R. E. (2001). Time-series analysis methods. In *Data analysis methods in physical oceanography* (p. 371).

European Union-Copernicus Marine Service. (2023). Global ocean gridded L 4 sea surface heights and derived variables reprocessed 1993 ongoing [Dataset]. *Mercator Ocean International*. https://doi.org/10.48670/moi-00148

Faure, V., & Speer, K. (2005). Labrador Sea water circulation in the northern North Atlantic Ocean. *Deep Sea Research Part II: Topical Studies in Oceanography*, *52*(3–4), 565–581. https://doi.org/10.1016/j.dsr2.2004.12.004

Fontela, M., García-Ibáñez, M. I., Hansell, D. A., Mercier, H., & Pérez, F. F. (2016). Dissolved organic carbon in the north Atlantic meridional overturning circulation. *Scientific Reports*, *6*(1), 1–9. https://doi.org/10.1038/srep26931

Fried, N., & de Jong, M. F. (2022). The role of the Irminger current in the Irminger Sea northward transport variability. *Journal of Geophysical Research: Oceans*, *127*(3), e2021JC018188. https://doi.org/10.1029/2021jc018188

Fu, Y., Lozier, S., Carrilho Bilo, T., Bower, A., Cunningham, S., Cyr, F., et al. (2023a). Meridional overturning circulation observed by the Overturning in the Subpolar North Atlantic Program (OSNAP) array from August 2014 to June 2020. [Dataset]. *Stl*. https://doi.org/10.35090/gatech/70342

Fu, Y., Lozier, S., Carrilho Bilo, T., Bower, A., Cunningham, S., Cyr, F., et al. (2023b). Seasonality of the meridional overturning circulation in the subpolar North Atlantic. *Communications Earth and Environment*, *4*(1), 181. https://doi.org/10.1038/s43247-023-00848-9

Hersbach, H., Bell, B., Berrisford, P., Hirahara, S., Horányi, A., Muñoz-Sabater, J., et al. (2020). The ERA5 global reanalysis. *Quarterly Journal of the Royal Meteorological Society*, *146*(730), 1999–2049. https://doi.org/10.1002/qj.3803

Holliday, N. P., Bacon, S., Cunningham, S., Gary, S., Karstensen, J., King, B., et al. (2018). Subpolar North Atlantic overturning and gyre-scale circulation in the summers of 2014 and 2016. *Journal of Geophysical Research: Oceans*, *123*(7), 4538–4559. https://doi.org/10.1029/2018jc013841

Hopkins, J., Holliday, N., Rayner, D., Houpert, L., Le Bras, I., Straneo, F., et al. (2019). Transport variability of the Irminger Sea deep western boundary current from a mooring array. *Journal of Geophysical Research: Oceans*, *124*(5), 3246–3278. https://doi.org/10.1029/2018jc014730

Jackson, L. C., Biastoch, A., Buckley, M. W., Desbruyères, D. G., Frajka-Williams, E., Moat, B., & Robson, J. (2022). The evolution of the North Atlantic meridional overturning circulation since 1980. *Nature Reviews Earth & Environment*, *3*(4), 241–254. https://doi.org/10.1038/s43017-022-00263-2

Käse, R. H., Biastoch, A., & Stammer, D. (2001). On the mid-depth circulation in the Labrador and Irminger Seas. *Geophysical Research Letters*, *28*(18), 3433–3436. https://doi.org/10.1029/2001gl013192

Lavender, K. L., Davis, R. E., & Owens, W. B. (2000). Mid-depth recirculation observed in the interior Labrador and Irminger Seas by direct velocity measurements. *Nature*, *407*(6800), 66–69. https://doi.org/10.1038/35024048

Le Bras, I.-A., Straneo, F., Holte, J., de Jong, M., & Holliday, N. (2020). Rapid export of waters formed by convection near the Irminger Sea's western boundary. *Geophysical Research Letters*, *47*(3), e2019GL085989. https://doi.org/10.1029/2019gl085989

Li, F., Lozier, M. S., Bacon, S., Bower, A., Cunningham, S., de Jong, M., et al. (2021). Subpolar North Atlantic western boundary density anomalies and the meridional overturning circulation. *Nature Communications*, *12*(1), 1–9. https://doi.org/10.1038/s41467-021-23350-2

Li, F., Lozier, M. S., & Johns, W. E. (2017). Calculating the meridional volume, heat, and freshwater transports from an observing system in the subpolar North Atlantic: Observing system simulation experiment. *Journal of Atmospheric and Oceanic Technology*, *34*(7), 1483–1500. https://doi.org/10.1175/jtech-d-16-0247.1

Locarnini, R., Mishonov, A., Antonov, J., Boyer, T., Garcia, H., Baranova, O., et al. (2013). Temperature. Vol. 1, world ocean atlas 2013. NOAA atlas nesdis 73 (p. 40).

Lozier, M. S., Li, F., Bacon, S., Bahr, F., Bower, A. S., Cunningham, S., et al. (2019). A sea change in our view of overturning in the subpolar North Atlantic. *Science*, *363*(6426), 516–521. https://doi.org/10.1126/science.aau6592

Medhaug, I., Langehaug, H. R., Eldevik, T., Furevik, T., & Bentsen, M. (2012). Mechanisms for decadal scale variability in a simulated Atlantic meridional overturning circulation. *Climate Dynamics*, *39*(1), 77–93. https://doi.org/10.1007/s00382-011-1124-z

Megann, A., Blaker, A., Josey, S., New, A., & Sinha, B. (2021). Mechanisms for late 20th and early 21st century decadal AMOC variability. *Journal of Geophysical Research: Oceans*, *126*(12), e2021JC017865. https://doi.org/10.1029/2021jc017865

Pickart, R. S., Straneo, F., & Moore, G. K. (2003). Is labrador sea water formed in the Irminger basin? *Deep Sea Research Part I: Oceanographic Research Papers*, *50*(1), 23–52. https://doi.org/10.1016/s0967-0637(02)00134-6

Pickart, R. S., Torres, D. J., & Fratantoni, P. S. (2005). The east Greenland spill jet. *Journal of Physical Oceanography*, *35*(6), 1037–1053. https://doi.org/10.1175/jpo2734.1

Piron, A., Thierry, V., Mercier, H., & Caniaux, G. (2017). Gyre-scale deep convection in the subpolar North Atlantic Ocean during winter 2014–2015. *Geophysical Research Letters*, *44*(3), 1439–1447. https://doi.org/10.1002/2016gl071895

Rogers, J. C. (1990). Patterns of low-frequency monthly sea level pressure variability (1899–1986) and associated wave cyclone frequencies. *Journal of Climate*, *3*(12), 1364–1379. https://doi.org/10.1175/1520-0442(1990)003<1364:polfms>2.0.co;2

Sabine, C. L., Feely, R. A., Gruber, N., Key, R. M., Lee, K., Bullister, J. L., et al. (2004). The oceanic sink for anthropogenic CO_2. *Science*, *305*(5682), 367–371. https://doi.org/10.1126/science.1097403

Spall, M. A., & Pickart, R. S. (2003). Wind-driven recirculations and exchange in the Labrador and Irminger Seas. *Journal of Physical Oceanography*, *33*(8), 1829–1845. https://doi.org/10.1175/2384.1

Srokosz, M., Baringer, M., Bryden, H., Cunningham, S., Delworth, T., Lozier, S., et al. (2012). Past, present, and future changes in the Atlantic meridional overturning circulation. *Bulletin of the American Meteorological Society*, *93*(11), 1663–1676. https://doi.org/10.1175/bams-d-11-00151.1

Straneo, F., Pickart, R. S., & Lavender, K. (2003). Spreading of Labrador Sea Water: An advective-diffusive study based on Lagrangian data. *Deep Sea Research Part I: Oceanographic Research Papers*, *50*(6), 701–719. https://doi.org/10.1016/s0967-0637(03)00057-8

Talley, L. D., & McCartney, M. S. (1982). Distribution and circulation of Labrador Sea Water. *Journal of Physical Oceanography*, *12*(11), 1189–1205. https://doi.org/10.1175/1520-0485(1982)012<1189:dacols>2.0.co;2

Thornalley, D. J., Oppo, D. W., Ortega, P., Robson, J. I., Brierley, C. M., Davis, R., et al. (2018). Anomalously weak Labrador Sea convection and Atlantic overturning during the past 150 years. *Nature*, *556*(7700), 227–230. https://doi.org/10.1038/s41586-018-0007-4

Våge, K., Pickart, R. S., Sarafanov, A., Knutsen, Ø., Mercier, H., Lherminier, P., et al. (2011). The Irminger gyre: Circulation, convection, and interannual variability. *Deep Sea Research Part I: Oceanographic Research Papers*, *58*(5), 590–614. https://doi.org/10.1016/j.dsr.2011.03.001

Våge, K., Spengler, T., Davies, H. C., & Pickart, R. S. (2009). Multi-event analysis of the westerly Greenland tip jet based upon 45 winters in ERA-40. *Quarterly Journal of the Royal Meteorological Society: A journal of the atmospheric sciences, applied meteorology and physical oceanography*, *135*(645), 1999–2011. https://doi.org/10.1002/qj.488

van Aken, H. M., de Jong, M. F., & Yashayaev, I. (2011). Decadal and multi-decadal variability of Labrador Sea water in the north-western North Atlantic Ocean derived from tracer distributions: Heat budget, ventilation, and advection. *Deep Sea Research Part I: Oceanographic Research Papers*, *58*(5), 505–523. https://doi.org/10.1016/j.dsr.2011.02.008

Yashayaev, I., Bersch, M., & van Aken, H. M. (2007). Spreading of the Labrador Sea Water to the Irminger and Iceland basins. *Geophysical Research Letters*, *34*(10), L10602. https://doi.org/10.1029/2006gl028999

Yeager, S., Castruccio, F., Chang, P., Danabasoglu, G., Maroon, E., Small, J., et al. (2021). An outsized role for the Labrador Sea in the multidecadal variability of the Atlantic overturning circulation. *Science Advances*, *7*(41), eabh3592. https://doi.org/10.1126/sciadv.abh3592

Zunino, P., Mercier, H., & Thierry, V. (2020). Why did deep convection persist over four consecutive winters (2015–2018) southeast of cape farewell? *Ocean Science*, *16*(1), 99–113. https://doi.org/10.5194/os-16-99-2020

Zweng, M. M., Reagan, J. R., Antonov, J. I., Locarnini, R. A., Mishonov, A. V., Boyer, T. P., et al. (2013). NOAA atlas NESDIS 74. In S. Levitus & A. Mishonov (Eds.), *World ocean atlas 2013, Salinity* (Vol. 2). NOAA Atlas NESDIS (Vol. 74).